Journal of Engineering Science and Technology
Vol. XX, No. Y (Year) PPP - QQQ

SYNTHESIS, CHARACTERISATION, AND FABRICATION HOLLOW FIBRES OF Zn-DOPED TiO_2 FOR DYE-SENSITIZED SOLAR CELLS

ZAINAL ARIFIN[1,2,*], SUDJITO SOEPARMAN[1], DENNY WIDHIYANURIYAWAN[1], AGUS PURWANTO[3], DHARMANTO[2]

[1]Department of Mechanical Engineering, Brawijaya University,
Jl. Mayjend. Haryono 167, Malang 65145, Indonesia
[2]Department of Mechanical Engineering, Sebelas Maret University,
Jl. Ir. Sutami 36 A, Surakarta 57126, Indonesia
[3]Department of Chemical Engineering, Sebelas Maret University,
Jl. Ir. Sutami 36 A, Surakarta 57126, Indonesia
*Corresponding Author: zainal_a@uns.ac.id

Abstract

The study aims to synthesize and characterize the hollow fibres of Zn-doped TiO_2. The hollow fibres were synthesized using a co-axial electrospinning machine where the sheath and core solution were composed of titanium (IV) isopropoxide and olive oil, respectively. Doping Zn was conducted by using zinc nitrate hexahydrate solution. The green fibres were then sintered at a temperature of 500°C. Subsequently, the hollow fibres of Zn-doped TiO_2 were fabricated as working electrode for dye-sensitized solar cells (DSSCs). The scanning electron microscopy images and X-ray diffraction analysis show that doping Zn produced the larger diameter and tuned the fraction of anatase and rutile of the hollow fibres of Zn-doped TiO_2. The best performance of DSSCs occurred at doping Zn into TiO_2 with a weight ratio of 0.4% where the respective open circuit voltage, current density, fill factor, and efficiency were 0.612 V, 2.935 mA/cm², 49.55%, and 0.89%. The main role of doping Zn into hollow fibres of TiO_2 for enhancing the performance of DSSCs was by increasing the current density caused by the larger diameter of hollow fibres of TiO_2 for dye loading and synergistic effect of anatase and rutile in the hollow fibres of TiO_2 for staging the electrons transfer.

Keywords: Hollow fibres, Co-axial electrospinning, Zn-doped TiO_2, Dye-sensitized solar cell.

Nomenclatures

B	Full width at half maximum, FWHM (rad)
D	Crystalline diameter (nm)
FF	Fill factor
IA	X-ray integrated intensities of the reflection of the anatase
I_{MPP}	Maximum power point current (mA)
IR	X-ray integrated intensities of the reflection of the rutile
I_{SC}	Short circuit current (mA)
J_{SC}	Short circuit current density (mA/cm^2)
k	Scherrer's constant, 0.9
V_{MPP}	Maximum power point voltage (V)
V_{OC}	Open circuit voltage (V)
X	Weight fraction of rutile (%)

Greek Symbols

λ	Wavelength of X-ray (1.5406 Å)
θ	Bragg angle (°)
η	Efficiency

Abbreviations

BET	Brunauer, Emmett and Teller
DSSCs	Dye-sensitized solar cells
FTO	Fluorine-doped tin oxide
SEM	Scanning electron microscopy
TiO_2	Titanium dioxide
TTIP	Titanium (IV) isopropoxide
TEM	Transmission electron microscopy
XRD	X-ray diffraction
Zn	Zinc
ZnO	Zinc oxide

1. Introduction

Dye sensitized solar cells (DSSCs) are the promising device for harvesting the solar energy because their operational cost is low and their performance is good enough when compared with solid-state photovoltaics. Although the operating principle of DSSCs is well understood, enhancing their performance is not an easy task since it is mutually influenced by many factors. Nowadays, various methods have been developed for exploring the knowledge of how to improve the performance of DSSCs. One of the important roles is using nano-sized semiconductor materials, particularly from anatase TiO_2 since they can produce a higher energy conversion efficiency when compared with that from rutile TiO_2 [1].

Furthermore, another method is carried out by producing a greater current density from DSSCs by means of simplifying and streamlining the movement of electrons. To do so, it used single-crystalline semiconductor nanowires, nanofibres, nanotubes arrays, and core-shell structure [2]. Of the various proposed strategies, nanofibres-shaped semiconductors produced via electrospinning are

very fascinating because of the ease of fabrication process with low cost [3-5]. Moreover, the repeatability and reproducibility of the fibres synthesized from the electrospinning machine was acceptable for the requirement of mass production [6]. Main parameters influencing the shape and the diameter of the nanofibres synthesized by electrospinning machine are solution concentration, solution viscosity, solution conductivity, molecular weight, solution rate, capillary size, working distance, and applied voltage [4, 7-11].

Interestingly again, the nanofibres semiconductor for DSSCs can be made in the form of a hollow to increase the dye uptake by using two coaxial capillaries electrospinning [12]. The solution used at the centre of the coaxial needle must have a lower volatility than that of the solution used at the outer side. The process of the formation of hollow fibres occurs by means of removing the core material by heating [13]. The hollow fibres are predicted to have a large surface area for increasing dyes adsorption onto TiO_2 semiconductors.

Furthermore, the goal of the semiconductor synthesizing does not only for improving the appropriate morphology but for increasing the electrical properties also. One of the methods to achieve such goal is using doping. Nitrogen and ytterbium doped into TiO_2 increased dipole moments and improved the photo-catalytic activity of TiO_2 [14]. Meanwhile, the doping of N-Zn producing 10-13 nm-sized TiO_2 particles improved the efficiency of the DSSCs to 2.6% [15]. The Fe doping at 0.28 wt% into the anatase TiO_2 has caused a partially shift of anatase TiO_2 (Eb = 3.0-3.1 eV) into rutile (Eb = 3.2 to 3.3 eV) [16]. Moreover, TiO_2 photo anode doped with Niobium (Nb) at 1 mol% showed a highest photovoltaic efficiency because they possessed the best band structure for DSSCs compared with that of vanadium (V)- and tantalum (Ta)-doped TiO_2 [17]. Furthermore, the 0.5 mol% ZnO-covered TiO_2 film possesses more outstanding ability to transport electrons leading to an increase of solar cells efficiency by 27.3% when compared with that of the pure TiO_2 (anatase) film [18]. The doping of magnesium into anatase TiO_2 has shifted the Fermi level 1 eV to a negative energy leading to increase the J_{sc} but to decrease the V_{oc} [19]. Meanwhile, the increase of TiO_2 electron mobility was maximum when doped by Zn of 0.1 mol% [20]. The aforementioned methods shows that the properties of the TiO_2 semiconductor resulted by doping are strongly depended by the type and concentration of dopant materials. The role for increasing electrical properties and enhancing the performance of DSSCs is manly by means of enhancing the current density rather than voltage. To this point of view, the Zn doping is interesting because it did not may control the TiO_2 particles size but increase the electron mobility also. Unfortunately, there are still limited studies of the employing Zn doping into TiO_2 hollow fibres for DSSCs. Therefore, we report here the synthesis and characterization of Zn-doped TiO_2 hollow fibres for improving the performance of the DSSCs.

2. Experimental Procedures

2.1. Synthesis and characterization of hollow fibres TiO_2 semiconductor

TiO_2 semiconductors were synthesized from the materials of titanium (IV) isopropoxide (TTIP, 99.9%, Sigma Aldrich-377996), polyvinylpyrolidone (PVP,

MW 40,000, Merck-PVP40), acetic acid (99.7%, Sigma Aldrich-320099), absolute ethanol (99.5%, Sigma Aldrich-459844). The materials were used without further purification. To prepare the precursor solution of electrospinning [21], 0.37 g of TTIP, 1.13 g of PVP, and 2 g of ethanol were mixed and stirred for 1 h. The acetic acid (0.78 g) was poured into the previous solution and then stirred for 11 h until transparence.

To prepare the solution for synthesizing the Zn-doped TiO_2, zinc nitrate hexahydrate (98%, Sigma Aldrich-228737) and acetic acid (0.78 g) were mixed and stirred for 12 h. The weight ratio between Zn and TiO_2 was controlled at 0.1, 0.4, 0.7, and 1.0%. Finally, the un-doped TTIP solution and the doped TTIP solution were ready for electrospinning.

To prepare the precursor solution for inner side (core) of hollow fibres, the olive oil (Sigma Aldrich-O1514) was stirred and heated at the temperature of 150°C by using magnetic stirrer for 4 h. This treatment was used for reducing the moisture content in the olive oil. The solution was then allowed to stand at a temperature of 25°C for 25 h until the foam and voids disappeared. Therefore, the olive oil solution was ready for electrospinning.

Synthesizing the fibres of TiO_2 was conducted by electrospinning machine showed in Fig. 1. The TTIP solution approximately 1 ml was put in the sheath of syringe pump. Meanwhile, the olive oil solution of 1 ml was poured into the core of syringe pump. The respective diameter of the core and the sheath needle is 0.3 mm and 0.8 mm. The needle of syringe pump and the FTO (fluorine-doped tin oxide) glass were then connected to the positive and the negative terminal of the high voltage, respectively. The distance between the tip of the syringe pump needle and the FTO glass was 29.5 cm, horizontally. The TTIP and olive oil solutions were then pushed out at a flow rate of 0.6 ml/h and 0.2 ml/h, respectively. When the electrospinning machine was subjected to a high voltage charge of approximately 15 kV, the solutions were then attracted by electrostatic fields towards the FTO glass. Firstly, the solutions were firstly formed into Taylor cone shape, followed by spinning into fibres shape, and finally the fibres attached on the surface of the collector called as green fibres.

The green fibres were then sintered at a temperature of 500°C for 2 h with a heating rate of 2.5°C/min. The hollow fibres of TiO_2 were produced when the solution of olive oil evaporated and the TTIP solution crystallized into TiO_2. Another objective of the sintering process was to decompose most of the organic materials including PVP and acetic acid.

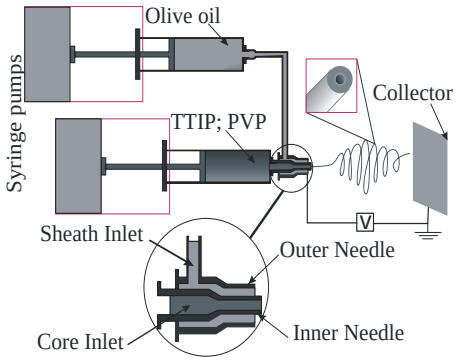

Fig. 1. Scheme of co-axial electrospinning machine.

The morphological features of the hollow TiO_2 fibres were examined using scanning electron microscopy (SEM, FEI: Inspect-S50). Phase analyses were carried out using X-ray Diffraction (XRD, Rigaku) with Cu-Kα radiation in the range of 20°–80° (2θ).

2.2. Fabricating and testing of DSSCs

To fabricate the DSSCs, fluorine-doped tin oxide (FTO) conducting glass substrates were first prepared using spray pyrolysis [22, 23]. Tin (II) chloride dihydrate (16.116 g, Cl_2Sn*2H_2O, Merck), ammonium fluoride (0.265 g, NH_4F, Merck), and ethyl alcohol (100 mL, 96%, Merck) were mixed and sprayed on the glass surface followed by heating at 450°C with a heating rate of 4°C/min.

To prepare the catalytic platinum counter electrode, the FTO glass was first heated at 200°C. Platinum was then chemically deposited, from a 5 mM H_2PtCl6 solution (Merck), onto the FTO glass followed by heating at 300°C and subsequent cooling with a cooling rate of 1°C/min. [24, 25].

To prepare the working electrode, the sintered hollow TiO_2 fibres were coated onto the FTO glass (1 cm × 1 cm) by the method of doctor blade. The resulting film-coated FTO glass was sintered at 450°C for 2 h [26, 27] to strongly adhere the hollow TiO_2 fibres onto the FTO glass [27, 28]. The thickness of the TiO_2 semiconductor film was maintained at 20 µm.

The electrolyte solution employed in the DSSCs was prepared as such: sodium iodide (3.30 g, 99.95%, Merck) was dissolved in 30 mL acetonitrile under stirring for 15 min, prior to adding iodine (523.88 g, 99.95%, Merck) and tungstophosphoric acid hydrate (5.48 mg, $H_3O_{40}PW_{12}{\cdot}xH_2O$, Merck). Stirring was continued for 24 h to achieve a homogeneous solution. The electrolyte solution was then injected into the assembled DSSCs spaced at 50 µm and then sealed. The voltage and current of DSSCs were recorded on a Keithley 2602A meter (USA) under illumination using a lamp of 1000 W/m². The fill factor and efficiency of the DSSC was determined from the open circuit voltage (V_{OC}), the short circuit current (J_{SC}), the maximum power point voltage (V_{MPP}), and the maximum power point current (I_{MPP}) as below.

$$FF = \frac{V_{MPP} \times I_{MPP}}{V_{OC} \times I_{SC}} \tag{1}$$

$$\eta = \frac{V_{MPP} \times I_{MPP}}{I_{light} \times A} \tag{2}$$

3. Results and Discussion

3.1. XRD characterization of Zn-doped hollow TiO_2 fibres

Fig. 2 shows the X-ray diffraction pattern of Zn-doped TiO_2. The peaks were detected at 2θ of 25.4°, 37.9°, 48.1°, 53.8°, and 55.0° assigned to the (101), (004), (200), (105), and (211) lattice planes corresponding to the TiO_2. The highest peak

of 25.4° (101) and 27.5° (110) showed the TiO_2 anatase and the TiO_2 rutile phase, respectively. Furthermore, the amount of anatase and rutile was calculated using the following equation [29, 30]:

$$X = \left(1 + 0.8\frac{IA}{IR}\right)^{-1} \tag{3}$$

Where, X is the weight fraction of rutile. IA and IR are the X-ray integrated intensities of the reflection of the anatase (101) and rutile (110). There are no ZnO diffraction peaks in the XRD spectra when Zn was doped at a weight ratio of Zn/TiO_2 up to 0.7% indicating that doping elements were well dispersed in TiO_2. At a weight ratio of Zn/TiO_2 of 1.0%, the ZnO diffraction peak was detected.

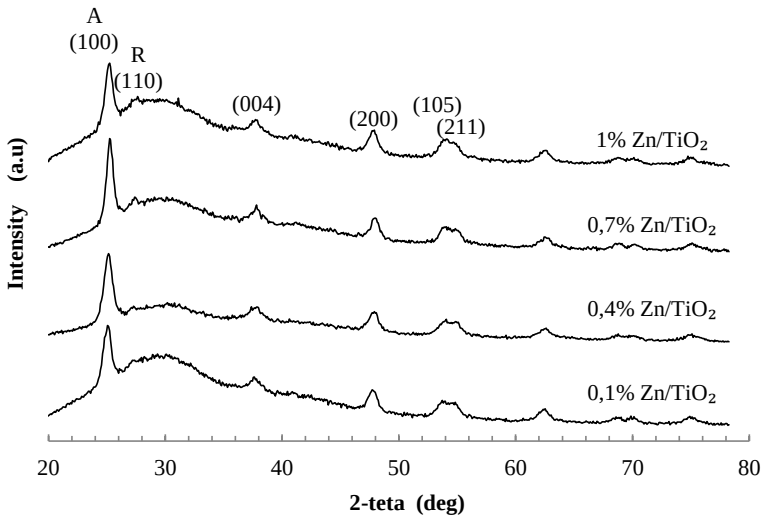

Fig. 2. X-ray diffraction pattern of Zn-doped TiO_2.

The diameter of crystallite hollow TiO_2 fibres was calculated by using Debye-Scherrer's equation based on the highest peak of 2θ at 25.4° [31]:

$$D = \frac{k.\lambda}{B.\cos\theta} \tag{4}$$

Where, D is the diameter of the crystallite TiO_2. λ is the wavelength of X-ray radiation (Cu Kα = 0.15406 nm). k is constant that is considered 0.9. θ is the angle of diffraction. B is the full width at the half-maximum intensity.

The crystallite diameter and the composition of anatase and rutile are shown in Table 1. The crystallite diameter of hollow TiO_2 fibres was varying from 8.07 to 10.41 nm. The main influence of Zn doping on the crystallite quality of hollow TiO_2 fibres was change the composition of the anatase and rutile phase. The highest weight fraction of anatase phase was 91% found at Zn/TiO_2 of 0.4%. Above 0.4%, the fraction of anatase was significantly reduced.

Table 1. The band gap energy and crystallite quality of hollow TiO_2 fibres.

Weight ratio of Zn/TiO_2 (%)	Band gap energy (eV)	Crystallite diameter (nm)	Composition (%)	
			Anatase	Rutile
0.1	3.24	8.99	84	16
0.4	3.24	8.07	91	9
0.7	3.25	10.41	86	14
1.0	3.25	9.40	82	18

Meanwhile, the band gap of hollow TiO_2 fibres calculated by Kubelka-Munk theory [32] was 3.24 eV to 3.25 eV. The Zn doping up to a weight ratio of 1.0% did not significantly change the band gap energy of hollow TiO_2 fibres. The band gap energy of hollow TiO_2 fibres was close to the previous study for hollow TiO_2 fibres, namely 3.21 [33].

3.2. Morphology of hollow fibres of Zn-doped TiO_2

Fig. 3 shows the morphology and size of hollow fibres TiO_2 after sintering at a temperature of 500°C for 2 h. The structures of hollow fibres are continuously connected without cracking. The size of the outer diameter of the hollow fibres was ranging from 192 nm to 314 nm, with an average fibre diameter of 221 nm. Meanwhile, the inner diameter of hollow fibres is not uniform ranging from 39 nm to 85 nm, with an average diameter of 65 nm.

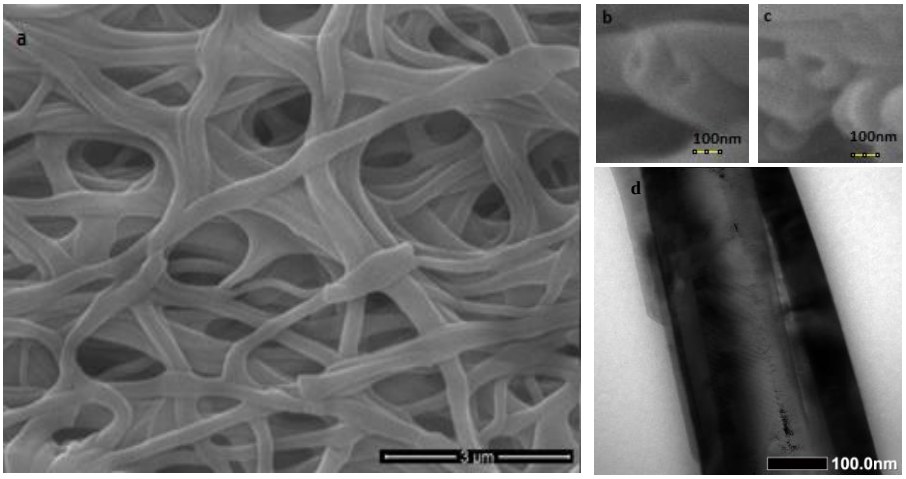

Fig. 3. SEM images of TiO_2 hollow fibres synthesized by coaxial electrospinning process followed by sintering at a temperature of 500°C for 2 h. (a) top view; (b) and (c) cross section; (d) TEM image

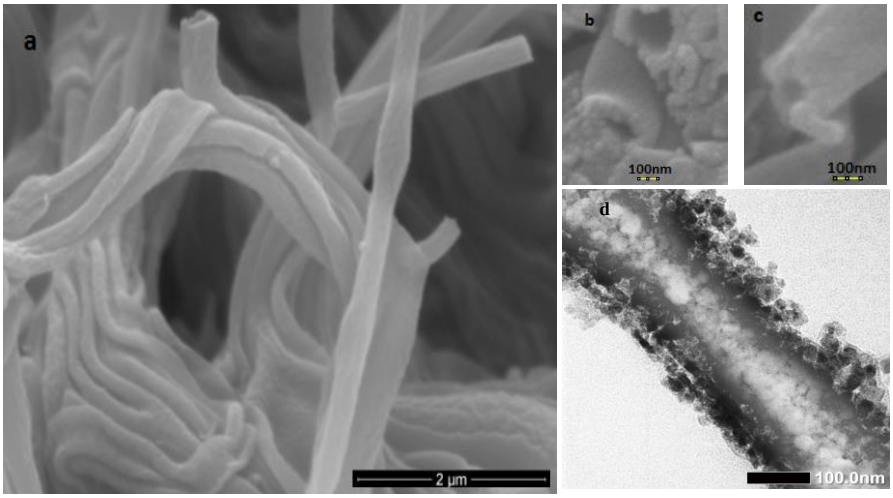

Fig. 4. SEM images of Zn-doped TiO_2 hollow fibres synthesized by coaxial electrospinning process followed by sintering at a temperature of 500°C for 2 h. (a) top view; (b) and (c) cross section; (d) TEM image.

Meanwhile, Fig. 4 shows that the morphology and size of Zn-doped TiO_2 hollow fibres after sintering at a temperature of 500°C for 2 h. The structure of the fibres is continuously connected without cracking. The size of the outer diameter of the hollow fibres is ranging from 245 nm to 328 nm, with an average diameter of 285 nm. Furthermore, the diameter of hollow fibres is not uniform, with hole sizes are ranging from 44 nm to 139 nm, with an average diameter of 91 nm. Thus, doping Zn into TiO_2 caused the increase of fibres diameter because the diameter of Zn^{2+} is larger than that of Ti^{4+}. Therefore, Zn is difficult to dope into the internal lattice of TiO_2 and forms Ti-O-Zn on the interface of the crystal TiO_2 [15]. This phenomenon was noted also by X-ray diffraction spectrum in Fig. 2 that the doping of Zn at 1% formed new phase of ZnO.

3.3. Performance of DSSCs

Fig. 5 show the photocurrent-voltage curve of DSSCs based on the hollow fibres of Zn-doped TiO_2 under irradiation intensity of 100 mW/cm^2, with the cell performances summarized in Table 2. The efficiency of the DSSC fabricated from the hollow and the solid TiO_2 fibres was 0.44% and 0.13%, respectively. The hollow fibres were capable to increase the efficiency of DSSCs up to four times when compared with that of the solid fibre-based DSSC. This significant increment of the efficiency in the hollow TiO_2 fibres-based DSSC was mainly caused by pores radius size and surface area. The hollow fibres of TiO_2 have a higher pores radius size and surface area than that of solid fibres of TiO_2. The respective pores radius size of solid and hollow TiO_2 fibres was 1.754 and 2.261 Å. BET measurement test results that the surface areas of TiO_2 solid fibres, TiO_2 hollow fibres and Zn-doped TiO_2 hollow fibres were 43.75, 65.95 and 86.75 m^2/g, respectively. Zn Doping on TiO_2 hollow fibres increase the value of the porosity of approximately 24% compared with TiO2 hollow fibres without doping. The

BET analisys of solid fibres found from this study was higher than that from the previous study (15.2 m^2/g) [34].

Table 2 shows also that the DSSCs with Zn-doped TiO_2 semiconductors produced similar V_{OC} approximately between 0.592 and 0.615 V. However, the J_{SC} of the DSSCs fabricated from Zn-doped TiO_2 was significantly influenced by Zn doping. The amount of J_{SC} and efficiency of DSSCs increased up to two fold when TiO_2 was doped by Zn up to the weight ratio of 0.4%. Over 0.4%, the amount of J_{SC} and efficiency of DSSCs experienced a sharp decline. Therefore, the optimum performance of DSSCs occurred by doping Zn into TiO_2 with a weight ratio of 0.4% where the respective V_{OC}, J_{SC}, *FF*, and efficiency were 0.612 V, 2.935 mA/cm^2, 49.55%, and 0.89%. This performance of DSSCs was higher than the previous study of DSSCs based on ZnO nanowires and N3 dye where V_{OC}, J_{SC}, and *FF* were 0.612 V, 1.029 mA, and 22.6% [35].

Therefore, the role of Zn doped into TiO_2 in improving the performance of solar cells occurred primarily by the improving the current density because Zn doping might increase the electron mobility [20]. In addition, the Zn doped into TiO_2 increasing the hole diameter of fibres in section 3.2 caused the increase the dye loading in the semiconductors. The Zn doping tuned also the fraction of anatase found in the hollow TiO_2 fibres as discussed in section 3.1. The optimum performance of DSSCs occurring with Zn doping at 0.4% indicated that there is a synergistic effect of anatase and rutile in the TiO_2 semiconductors for enhancing the performance of DSSCs. The anatase posesses an indirect band gap semiconductor. In the indirect band gap material, the minimum in the conduction band is away from the maximum in the valence band. This enables the excited electron to stabilize at the lower level in the conduction band. Because the properties of indirect band gap material, so that it minimizes the recombination effect in DSSCs [36]. This results were consistent with the previous study that the strongest synergistic effect between the anatase and rutile phases occurred in the DSSCs with rutile fraction of 13 wt% [1]. At this fraction of rutile, the staging of band gap energy between anatase and rutile was the best and caused the easier transfer of electrons from rutile to anatase in DSSCs. The indirect band gap enables the excited electron to stabilize at the lower level in the conduction band itself leading to its longer life and greater mobility [36]. Further addition of rutile might trigger accelerated interception of injected electrons by the electrolyte, resulting in decreased current density and photo voltage [1].

Table 2. The performance of DSSCs

Weight ratio of Zn/TiO_2 (%)	Fibres	V_{OC} (V)	J_{SC} (mA/cm^2)	*FF* (%)	η (%)
0	Solid	0.604	0.419	51.39	0.13
0	Hollow	0.592	2.136	34.61	0.44
0.1	Hollow	0.615	2.506	55.56	0.86
0.4	Hollow	0.612	2.935	49.55	0.89
0.7	Hollow	0.609	1.599	42.90	0.42
1.0	Hollow	0.601	1.384	47.80	0.40

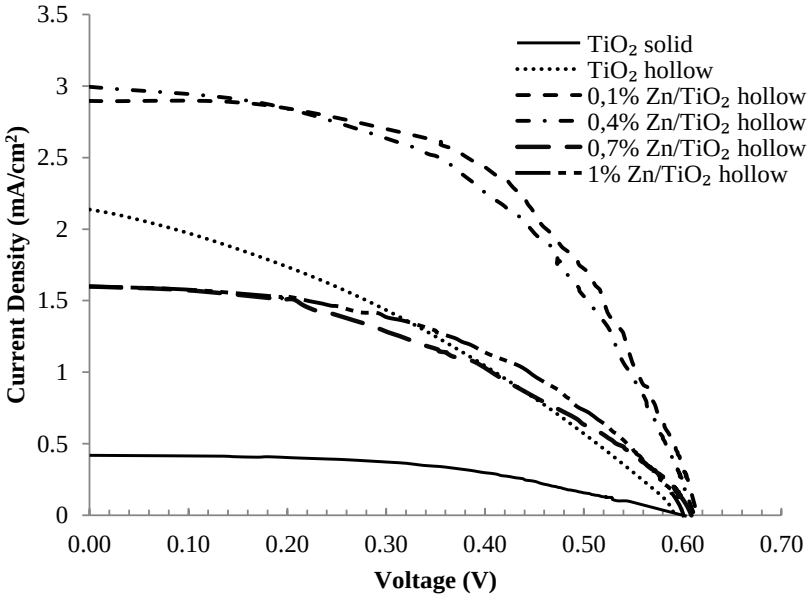

Fig. 5. The photocurrent-voltage curve of DSSCs under irradiation intensity of 100 mW/cm^2

4. Conclusions

The method of fabricating hollow TiO_2 fibres semiconductor and Zn doping into TiO_2 fibres by using coaxial electrospinning has been successfully carried out. The Zn doping produced the larger diameter of hollow TiO_2 fibres. In addition, the Zn doping has tuned the fraction of anatase and rutile in the hollow fibres of TiO_2. In contrast, the Zn doping did not significantly change the crystallite diameter and band gap energy. The best performance of DSSCs occurred by doping Zn into TiO_2 with a weight ratio of 0.4% where the respective V_{OC}, J_{SC} , *FF*, and efficiency were 0.612 V, 2.935 mA/cm², 49.55%, and 0.89%. The main role of Zn doping into hollow TiO_2 fibres for enhancing the performance of DSSCs was by increasing the current density caused by the larger diameter of hollow TiO_2 fibres for dye loading and the synergistic of anatase and rutile in the hollow TiO_2 fibres for staging the electrons transfer. Further study is needed to optimize the surface area and the diameter of hollow TiO_2 fibres for DSSCs by tuning the flow rate of core and sheath solutions in the electrospinning. It is interesting also to study further the method of synthesizing the uniform fibres from the electrospinning.

Acknowledgements

The authors thank to the Rector of Sebelas Maret University (UNS) and DP2M DIKTI for the financial support through the research grant Nr. 624/UN27.11/PL/2015.

References

1. Li, G.; Richter, C.P.; Milot, R.L.; Cai, L.; Schmuttenmaer, C.A.; Crabtree, R.H.; Brudvig, G.W.; and Batista, V.S. (2009). Synergistic effect between anatase and rutile TiO_2 nanoparticles in dye-sensitized solar cells, *Dalton Transactions*, 45(45), 10078-10085.
2. Kim, I.D.; Hong, J.M.; Lee, B.H.; Kim, D.Y.; and Jeon, E.K. (2007). Dye-sensitized solar cells using network structure of electrospun ZnO nanofiber mats, *Applied Physics Letters*, 91(16), 163109.
3. Dong, Z.; Kennedy, S.J.; and Wu, Y. (2011). Electrospinning materials for energy-related applications and devices, *Journal of Power Sources*, 196(11), 4866-4904.
4. Ren, H.; Ding, Y.; Jiang, Y.; Xu, F.; Long, Z.; and Zhang, P. (2009). Synthesis and properties of ZnO nanofibers prepared by electrospinning, *Sol-Gel Science Technology*, 52(2), 287-290.
5. Suyitno; Purwanto, A.; Hidayat, R.L.L.G.; Sholahudin, I.; Yusuf, M.; Huda, S.; and Arifin, Z. (2014). Fabrication and characterization of zinc oxide-based electrospun nanofibers for mechanical energy harvesting, *Journal of Nanotechnology in Engineering and Medicine*, 5(1), 011002.
6. Suyitno; Huda, S.; Arifin, Z.; Hadi, S.; and Lambang, R.L. (2014), Repeatability and reproducibility of fibre-based nanogenerator synthesized by electrospinning machine, *IOP Conference Series: Materials Science and Engineering*, 58(1), 012013.
7. Pham, Q.P.; Sharma, U.; and Mikos, A.G. (2006). Electrospinning of polymeric nanofibers for tissue engineering applications: a review, *Tissue Engineering*, 12(5), 1197-1211.
8. Park, J.Y.; and Kim, S.S. (2009). Growth of Nanograins in Electrospun ZnO Nanofibers, *The American Ceramic Society*, 92(8), 1691-1694.
9. Park, J.A.; Moon, J.; Lee, S.J.; Lim, S.C.; and Zyung, T. (2009). Fabrication and characterization of ZnO nanofibers by electrospinning, *Current Applied Physics*, 9(3), 210-212.
10. Baek, J.H.; Park, J.; Kang, J.; Kim, D.; Koh, S.W.; and Kang, Y.c. (2012). Fabrication and thermal oxidation of ZnO nanofibers prepared via electrospinning technique, *Bulletin Korean Chemical Society*, 33(8), 2694-2698.
11. Sangkhaprom, N.; Supaphol, P.; and Pavarajarn, V. (2010). Fibrous zinc oxide prepared by combined electrospinning, *Ceramics International*, 36(1), 357-363.
12. McCann, J.T.; Li, D.; and Xia, Y. (2005). Electrospinning of nanofibers with core-sheath, hollow, or porous structures, *Journal of Materials Chemistry*, 15(7), 735–738.
13. Samadpour, M.; Gimenez, S.; Zad, A.I.; Taghavinia, N.; and Mora-Sero, I. (2011). Easily manufactured TiO_2 hollow fibers for quantum dot sensitized solar cells, *Physical Chemistry Chemical Physics*, 14(2), 522–528.
14. Pan, G.; Xuejun, Z.; Wenfang, Z.; Jing, W.; and Qingju, L. (2010). First-principle study on anatase TiO2 codoped with nitrogen and ytterbium, *Journal of Semiconductors*, 31(3), 032001.
15. Hai, F.Z.; Chang, Z.J.; Ying, Y.X.; and Liang, C.W. (2011). Preparation of nano-crystal N–Zn/TiO_2 anode films and the effects of co-sensitization on the performance of dye-sensitized solar cells, *Chinese Science Bulletin*, 56(19), 2001–2008.

16. Ranjit, K.T.; and Viswanathan, B. (1997). Synthesis, characterization and photocatalytic properties of iron-doped TiO_2 catalysts *Journal of Photochemistry and Photobielogy A: Chemistry*, 108(1), 79-84.
17. Liu, J.; Duan, Y.; Zhou, X.; and Lin, Y. (2013). Influence of V_B group doped TiO_2 on photovoltaic performance of dye-sensitized solar cells, *Applied Surface Science*, 277(1), 231– 236.
18. Wang, Z.S.; Huang, C.H.; Huang, Y.Y.; Hou, Y.J.; Xie, P.H.; Zhang, B.W.; and Cheng, H.M. (2001). A Highly Efficient Solar Cell Made from a Dye-Modified ZnO-Covered TiO_2 Nanoporous Electrode, *Chemistry of Materials*, 13(2), 678-682.
19. Nam, T.V.; Trang, N.T.; and Cong, B.T. (2012). Mg-doped TiO_2 for dye-sensitive solar cell: an electronic structure study, *Proc. Natl. Conf. Theor. Phys.*, 37(2), 233-242.
20. Yeo, M.-K.; and Kang, M. (2010). The effect of nano-scale Zn-doped TiO_2 and pure TiO_2 particles on Hydra magnipapillata, *Molecular & Cellular Toxicology*, 6(1), 9-17.
21. Song, M.Y.; Ahn, Y.R.; Jo, S.M.; and Kim, D.Y. (2005). TiO_2 single-rystalline nanorod electrode for quasi-solod-state dye-sensitized solar cells, *Applied Physics Letters*, 87(11), 113113.
22. Moholkar, A.V.; Pawar, S.M.; Rajpure, K.Y.; Bhosale, C.H.; and Kim, J.H. (2009). Effect of fluorine doping on highly transparent conductive spray deposited nanocrystalline tin oxide thin films, *Applied Surface Science*, 255(23), 9358–9364.
23. Suyitno; Arifin, Z.; Santoso, A.A.; Setyaji, A.T.; and Ubaidillah (2014). Optimization Parameters and Synthesis of Fluorine Doped Tin Oxide for Dye-Sensitized Solar Cells, *Applied Mechanics and Materials*, 575, 689-695.
24. Calandra, P.; Calogero, G.; Sinopoli, A.; and Gucciardi, P.G. (2010). Metal nanoparticles and carbon-based nanostructures as advanced materials for cathode application in dye-sensitized solar cells, *International Journal of Photoenergy*, 2010, 109495.
25. Suyitno, S.; Saputra, T.J.; Supriyanto, A.; and Arifin, Z. (2015). Stability and efficiency of dye-sensitized solar cells based on papaya-leaf dye, *Spectrochimica Acta - Part A: Molecular and Biomolecular Spectroscopy*, 148, 99-104.
26. Wongcharee, K.; Meeyoo, V.; and Chavadej, S. (2007). Dye-sensitized solar cell using natural dyes extracted from rosella and blue pea flowers, *Solar Energy Materials and Solar Cells*, 91(7), 566-571.
27. Chang, H.; Wu, H.M.; Chen, T.L.; Huang, K.D.; Jwo, C.S.; and Lo, Y.J. (2010). Dye-sensitized solar cell using natural dyes extracted from spinach and ipomoea, *Journal of Alloys and Compounds*, 495(2), 606–610.
28. Chang, H.; and Lo, Y.J. (2010). Pomegranate leaves and mulberry fruit as natural sensitizers for dye-sensitized solar cells, *Solar Energy*, 84(10), 1833–1837.
29. Bakardjieva, S.; Subrt, J.; Sˇtengl, V.c.; Dianez, M.J.; and Sayagues, M.J. (2005). Photoactivity of anatase–rutile TiO_2 nanocrystalline mixtures obtained by heat treatment of homogeneously precipitated anatase, *Applied Catalysis B: Environmental*, 58(3-4), 193–202.
30. Pei, C.C.; and Leung, W.W.-F. (2013). Enhanced photocatalytic activity of electrospun TiO_2/ZnO nanofibers with optimal anatase/rutile ratio, *Catalysis Communications*, 37, 100–104.
31. Pongwan, P.; Inceesungvorn, B.; and Wetchakun, K. (2012). Highly efficient visible-light-induced photocatalytic activity of Fe-doped TiO_2 nanoparticles *Engineering Journal*, 16(3), 143-151.

32. Murphy, A.B. (2007). Band-gap determination from diffuse reflectance measurements of semiconductor films, and application to photoelectrochemical water splitting, *Solar Energy Materials and Solar Cells*, 91(14), 1326–1337.
33. Chang, W.; Xu, F.; Mu, X.; Ji, L.; Ma, G.; and Nie, J. (2013). Fabrication of nanostructured hollow TiO_2 nanofibers with enhanced photocatalytic activity by coaxial electrospinning, *Chemical Science*, 3(4), 1262-1272.
34. He, G.; Cai, Y.; Zhao, Y.; Wang, X.; Lai, C.; Xi, M.; Zhu, Z.; and Fong, H. (2013). Electrospun anatase-phase TiO_2 nanofibers with different morphological structures and specific surface areas, *Journal of Colloid and Interface Science*, 398, 103–111.
35. Zhitao, H.; Sisi, L.; Junjun, L.; Jinkui, C.; and Yong, C. (2013). Facile synthesis of ZnO nanowires on FTO glass for dye-sensitized solar cells, *Journal of Semiconductors*, 34(7), 074002.
36. Banerjee, S., Gopal, J., Muraleedharan, P., Tyagi, A.K., and Raj1, B. (2006). Physics and chemistry of photocatalytic titanium dioxide: visualization of bactericidal activity using atomic force microscopy, *Current Science*, 90, 1378-1383